Dynamic structures in shock-loaded copper

Yu. I. Meshcheryakov, A. K. Divakov, N. I. Zhigacheva, I. P. Makarevich, and B. K. Barakhtin*
Institute of Problems of Mechanical Engineering, Russian Academy of Sciences, Saint Petersburg, Russia
(Received 6 March 2008; revised manuscript received 25 June 2008; published 1 August 2008)

Shock loading of polycrystalline copper under uniaxial strain conditions at 6.2÷7.3 GPa results in nucleating the dissipative structures of 5÷25 μm in diameter. Interior of each structure is a network of microshear bands of 100÷300 nm spacing. Nucleation of structures occurs at the impact velocity where particle velocity dispersion begins to grow faster than mean particle velocity or when the local strain rate at the mesoscale becomes higher than the macroscopic strain rate. Simultaneously, defect of particle velocity at the plateau of compressive pulse, macrohardness, and spall strength grow in the same manner. Physically, nucleation of dissipative structures is estimated to be initiated under resonance condition between space periods of polarized dislocation structure and driving plastic front.

DOI: 10.1103/PhysRevB.78.064301 PACS number(s): 62.50.−p, 61.82.Rx, 67.25.dk

I. INTRODUCTION

Mechanisms of heterogeneity of dynamic straining within wide range of pressures, strain rates, and durations of loading pulse is a subject of intensive study for several decades.[1–8] Recent review of Murr and Esquivel[9] designates three basic mechanisms for heterogeneity at high strain rates: (a) shear banding, (b) twinning, and (c) dynamic recrystallization. Reaction of internal structure on impact was found to depend on (i) stacking fault energy, (ii) critical twinning pressure, (iii) grain size, (iv) strain rate, and (v) scheme of shock loading. These factors are shown to determine a slip twining transition in dynamically deformed solids.

Enumerated mechanisms of heterogeneity are known to be grounded on driven motion of dislocations. In parallel, the shock induced turbulence and rotational mechanisms of dynamic plasticity are studied both experimentally and theoretically.[10–13] The turbulence in shock compressed media is thought to play a key role in the problem of inertial thermonuclear synthesis.[14] The second approach supposes that dynamic deformation of solids flows in hydrodynamic regime as a convective process under conditions of "high pressure plus shear" similar to that realized in Bridgman chamber. Whereas dislocation sliding and twinning are considered to play an accommodative function. In this connection, the main objective of paper is to reveal whether the shock induced turbulence in solids is of pure hydrodynamic nature—so the presence of crystalline lattice may be ignored—or dislocation dynamics, shear banding, and twinning are incorporated into rotational motion in crystalline solid as natural mechanisms for the shock induced turbulence to be realized. Additional motivation for our work is the experimental conformation of simulation of shock induced turbulence in copper in Ref. 12 (see Fig. 1). Although very visual, the results of modeling do not reflect an effect of fcc crystalline lattice on internal structure of eddies. Their displacement fields are of circlelike trajectories, which is physically impossible because the sliding can flow only in crystalline planes. In the very beginning of 1990s, the analogous question on the mechanism of anomalous elongation of shape charge jets has been raised. This mechanism was shown to be the dynamic recrystallization,[15,16] which is certainly the solid-state mechanism of deformation although outwardly the shape charge jet elongation looks as a pure hydrodynamic phenomenon.

II. EXPERIMENT TECHNIQUE

Shock loading of plane *M*3 copper targets of 52 mm in diameter and 5-mm thick under uniaxial strain conditions was conducted by using a 37-mm bore diameter one stage light gas gun, which accelerates impactor to velocity of 100÷1000 m/s. Preventing reloading is a primary requirement because the structure after impact is to be interpreted due to the single loading. Effects of reflected waves are minimized by using a longitudinal momentum trap.[17,18] To conserve the structure state created by shock loading, 25-mm plug targets of studied material were conically pressed inside the 52-mm copper rings.[19] This allows to eliminate a passing of lateral waves through the material of interest. In part of tests, behind the target an additional copper plate of 2.5-mm thick was mounted. With a proper ratio of target to plate thickness, interaction between rarefaction from the free surface of the target with the release wave originating at the rear surface of impactor happens at the target plate boundary resulting in the so-called "artificial spallation."

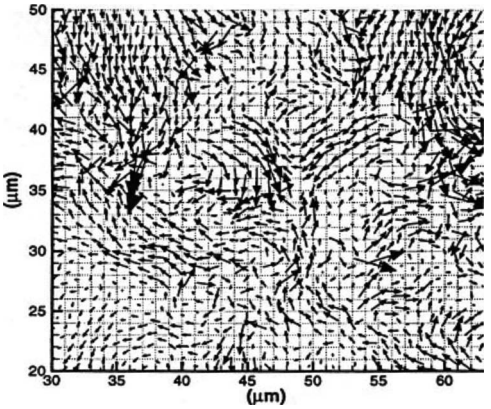

FIG. 1. Displacement field of rotation cell in copper [after (Ref. 12)].

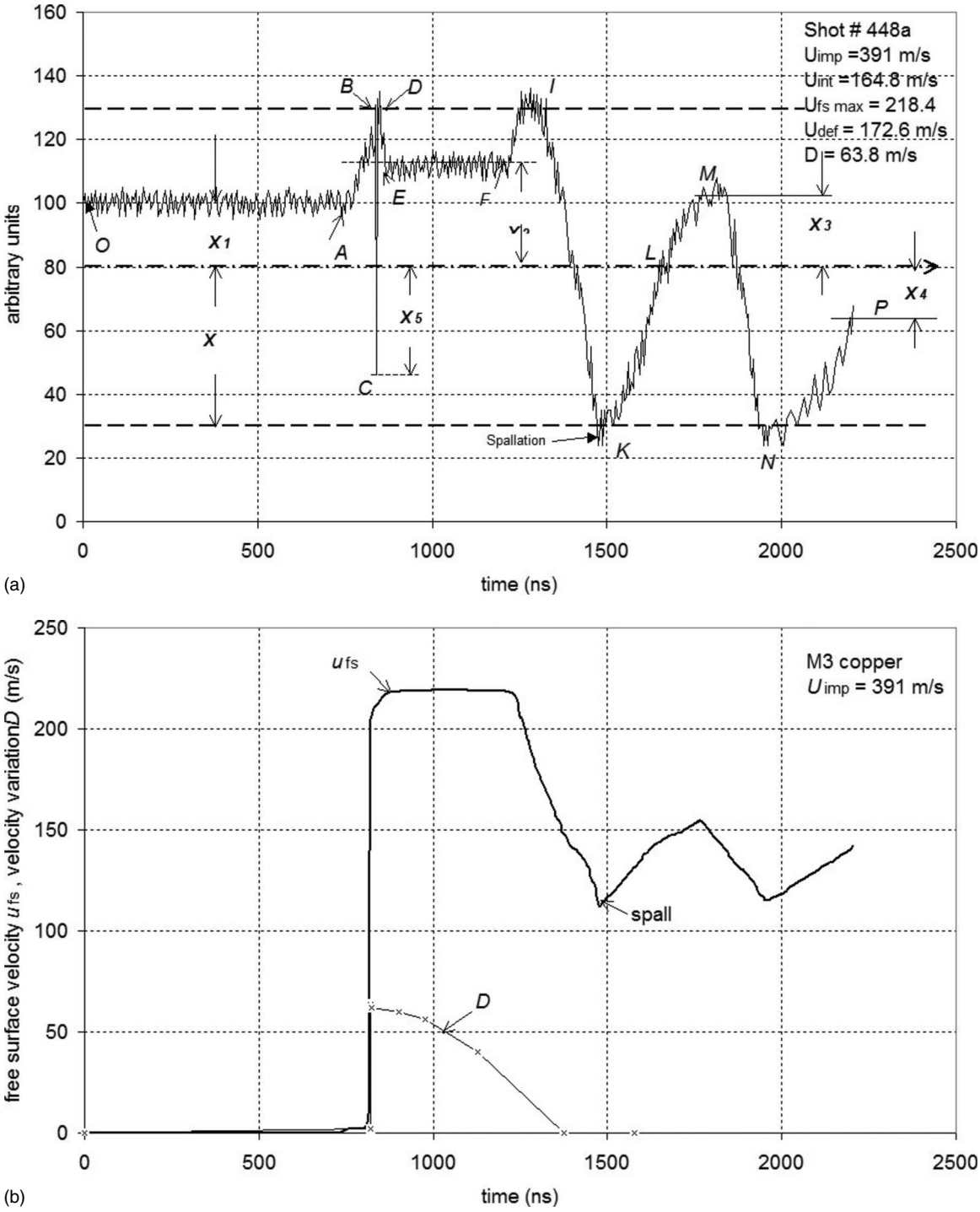

FIG. 2. Fringe signal (a) and deciphered free-surface profiles for mean particle velocity and velocity variation (b) for a 5-mm copper target loaded at impact velocity of 391 m/s.

To verify the intensity of particle velocity fluctuations as a quantitative characteristics of nonuniformity of dynamic straining, a measuring of the particle velocity variation was conducted.[20] In our experiments, for measuring the velocity variation a modified two channel Sandia interferometer was used.[21] For registering the fringe signals, "Hamamatsu" photomultipliers of 0.6-ns transient characteristics and "Tektroniks-3054" digital oscilloscope of 500 Mc bandwidth were used, which together with the properly chosen delay time of interferometer provides a temporal resolution of the order of one nanosecond. Value of interferometer constant U_{int}, which is determined by the delay shoulder of interferometer, was varied. So, at the impact velocity of U_{imp} $=170.4$ m/s interferometer constant equals 74 m/s per fringe, whereas at higher impact velocities the interferometer constant was taken to be 164.8 or 280.1 m/s per fringe. In Fig. 2(a), as example, fringe signal for impact velocity of $U_{\text{imp}}=391$ m/s is provided ($U_{\text{int}}=164.8$ m/s per fringe).

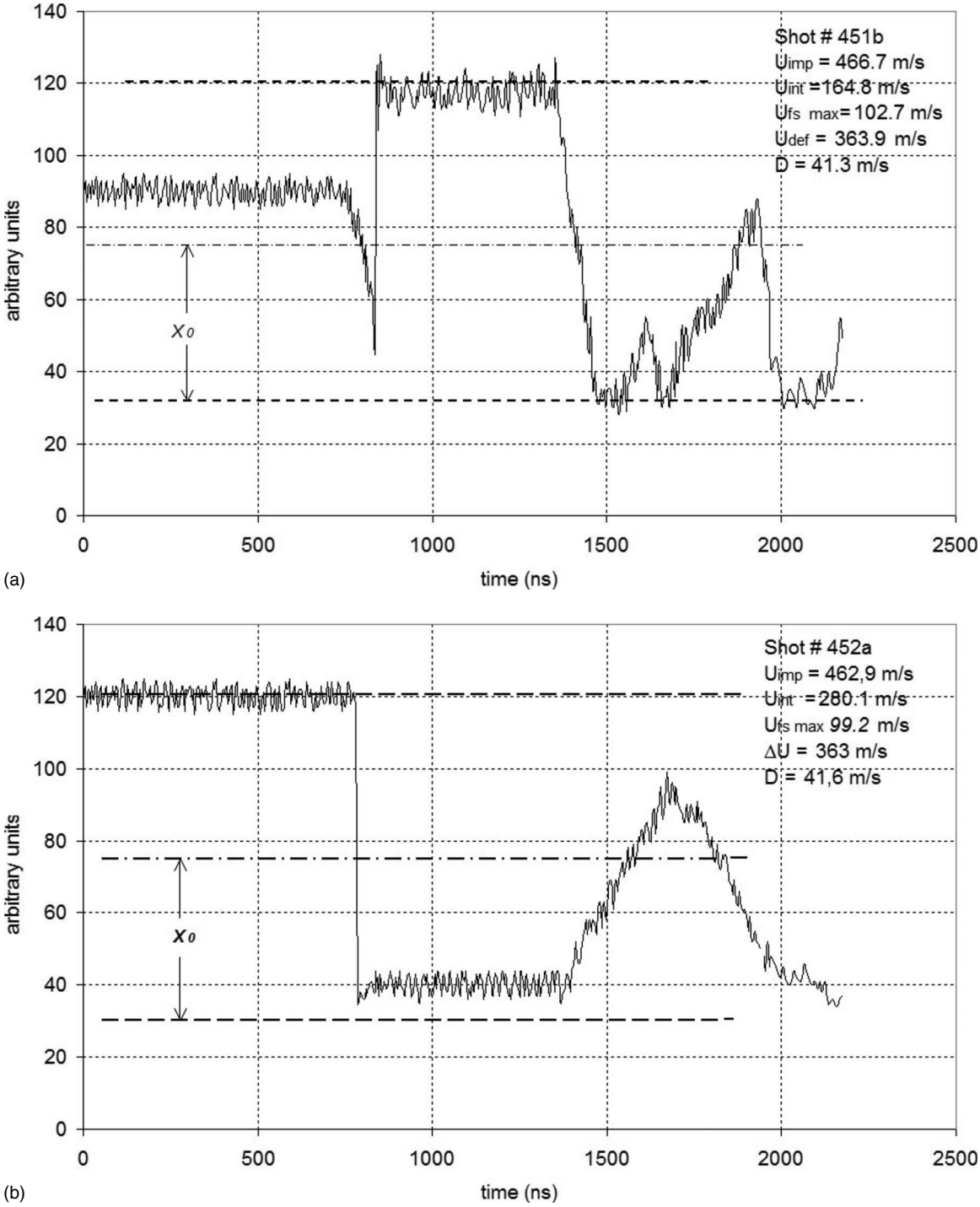

FIG. 3. Fringe signals for a 5-mm copper targets loaded at impact velocity of 466.7 m/s (interferometer constant $U_{\text{int}}=164.8$ m/s per fringe) and 462.9 m/s (interferometer constant $U_{\text{int}}=280.1$ m/s per fringe).

The fringe signal is subdivided by several pieces. Appearance of shock front corresponds to position A, where $U_{\text{fs}}=0$. According to rules for the deciphering of interference signals,[21,22] the values of free-surface velocity corresponding to each piece are determined as follows:

$$U_{\text{fs}}^{AB} = \frac{U_{\text{int}}}{4} - U_{X_1} = 41.2 - U_{X_1} = 30.6 \text{ m/s},$$

$$U_{X_1} = \frac{U_{\text{int}}}{2\pi}\arcsin\frac{X_1}{X_0} = 26.23 \arcsin 0.4 = 26.23 \cdot 0.414 = 10.6 \text{ m/s}.$$

Here X_0 is the maximum amplitude of fringe signal and X_1 is the amplitude of fringe signal corresponding to piece AB [see Fig. 2(a)].

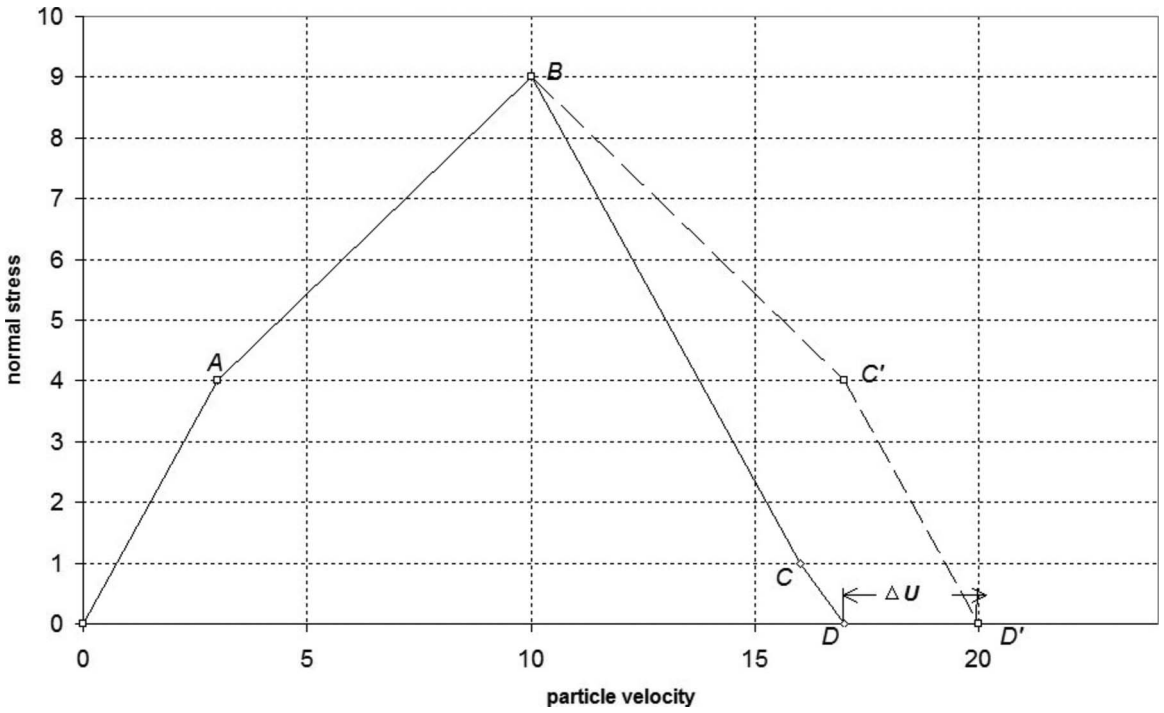

FIG. 4. Normal stress—particle velocity diagram for strain rate independent material.

$$U_{\mathrm{fs}}^{BCD} = U_{\mathrm{int}} = 164.8 \ \mathrm{m/s\ (one\ \ fringe)}.$$

$$U_{\mathrm{fs}}^{DE} = \frac{U_{\mathrm{int}}}{4} - U_{X_2}, \quad U_{X_2} = \frac{U_{\mathrm{int}}}{2\pi}\arcsin\frac{X_2}{X_0} = 18.17 \ \mathrm{m/s}.$$

$$U_{\mathrm{fs}}^{DE} = 41.2 - 18.17 = 23.03 \ \mathrm{m/s}.$$

Thus, the peak value of the free-surface velocity equals:

$$U_{\mathrm{fs}}^{\max} = U_{\mathrm{fs}}^{AB} + U_{\mathrm{fs}}^{BCD} + U_{\mathrm{fs}}^{DE} = 30.6 + 164.8 + 23.03 = 218.43 \ \mathrm{m/s}.$$

Along piece *EF* the free-surface velocity is invariable. Value of the free-surface velocity at the release front of compressive pulse equals:

$$U_{\mathrm{fs}}^{FI} = U_{\mathrm{fs}}^{DE} = 23.03 \ \mathrm{m/s},$$

$$U_{\mathrm{fs}}^{IK} = \frac{U_{\mathrm{int}}}{2} = 82.4 \ \mathrm{m/s},$$

$$U_{\mathrm{fs}}^{KL} = \frac{U_{\mathrm{int}}}{4} = 41.2 \ \mathrm{m/s},$$

$$U_{\mathrm{fs}}^{LM} = \frac{U_{\mathrm{int}}}{2\pi}\arcsin\frac{X_3}{X_0} = 11.72 \ \mathrm{m/s},$$

$$U_{\mathrm{fs}}^{MN} = U_{\mathrm{fs}}^{KL} + U_{\mathrm{fs}}^{LM} = 52.92 \ \mathrm{m/s},$$

$$U_{\mathrm{fs}}^{NP} = \frac{U_{\mathrm{int}}}{4} - \frac{U_{\mathrm{int}}}{2\pi}\arcsin\frac{X_4}{X_0} = 32.07 \ \mathrm{m/s}.$$

Deficit of the free-surface velocity at the top of compressive pulse equals:

$$\Delta U = U_{\mathrm{imp}} - U_{\mathrm{fs}}^{\max} = 391 - 218.43 = 172.57 \ \mathrm{m/s}.$$

Spallation happens in position *K*, so the value of pull back velocity corresponding spallation equals:

$$U_{\mathrm{fs}}^{p-b} = U_{\mathrm{fs}}^{FI} + U_{\mathrm{fs}}^{IK} = 105.43 \ \mathrm{m/s}.$$

The second dynamic variable, which characterizes a response of material on impact is the particle velocity dispersion, D^2—which results from the particle velocity inhomogeneity during the shock propagation through the material. When monitored with laser interferometer, different mesoparticles within laser spot at the free surface of target— because of particle velocity scattering—give different Doppler shifts of laser radiation, which leads to partial loss of interference contrast of reflected beam. Herewith, amplitude of fringe signal decreases as compared to situation when laser beam of interferometer reflects from the perfect surface. In Fig. 2(a) maximum decrease in fringe signal corresponds to position ***C***. Interference contract equals ratios of current signal amplitude and maximum amplitude of fringe signal, $K = X_5/X_0$. Maximum value of velocity variation, *D*, (square root of the particle velocity dispersion) can be determined by using formulas:[21,22]

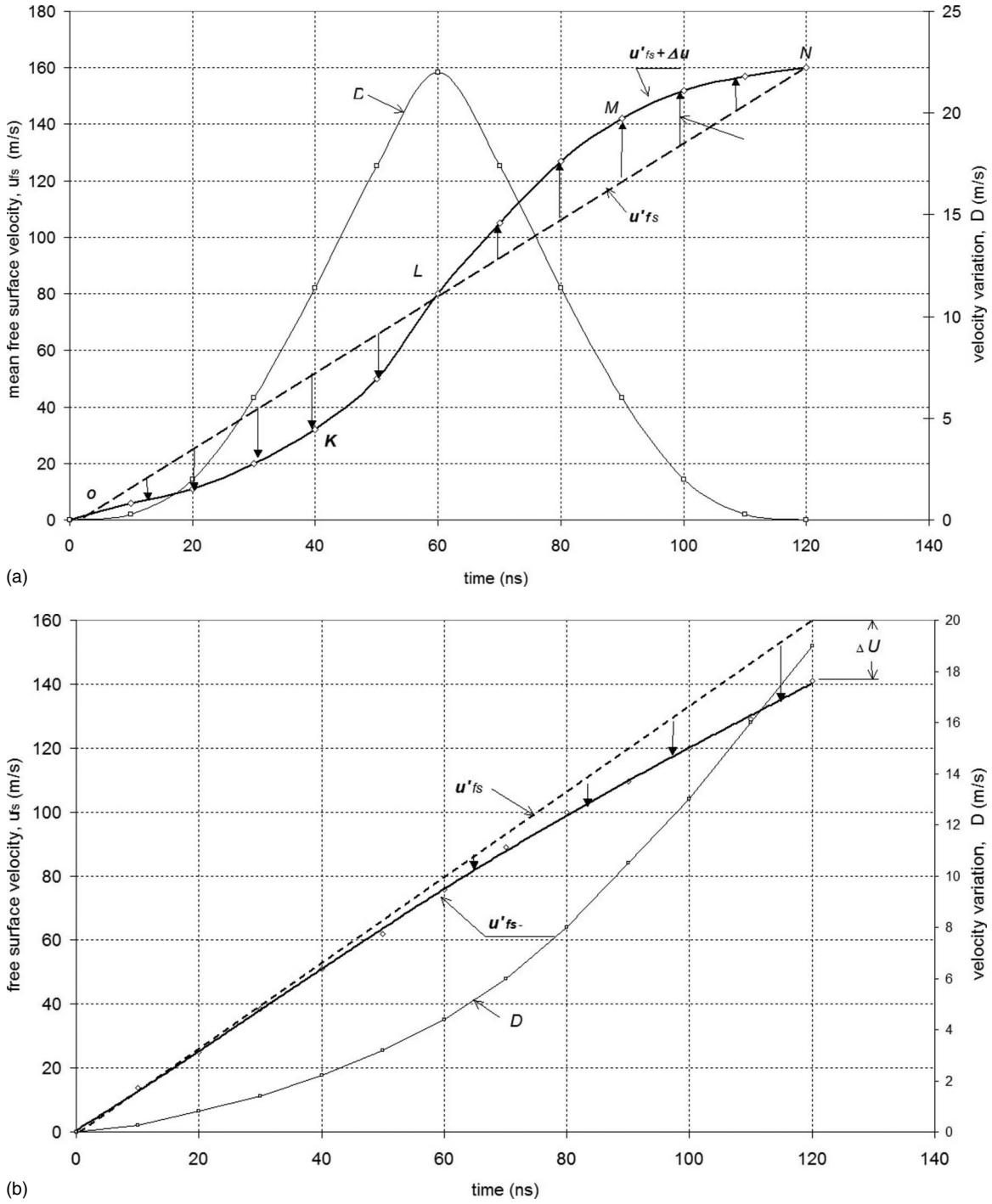

FIG. 5. Qualitative picture of momentum exchange between mean particle velocity and particle velocity dispersion for (a) steady shock front and (b) unsteady front.

$$K = \exp\left(-\frac{\pi^2 D^2}{2U_{\text{int}}^2}\right) \quad \text{or} \quad D = \frac{U_{\text{int}}}{\pi}\sqrt{-2\ln K}.$$

In accordance with Fig. 2(a), at the impact velocity of 391 m/s the value of fringe contrast $K = X_5/X_0 = 0.702$. So the velocity variation $D = 164.8/\pi\sqrt{-2\ln 0.702} = 63.38$ m/s.

Deciphered free-surface velocity profiles for mean particle velocity and for velocity variation are provided in Fig. 2(b).

Two shots were performed with different interferometer constant values: one shot with interferometer constant $U_{\text{int}} = 164.8$ m/s per fringe (delay time $\tau_d = 1.92$ ns) and another with $U_{\text{int}} = 280.1$ m/s per fringe ($\tau_d = 1.13$ ns). This was done to make sure that the measured value of particle velocity does not depend on interferometer constant. Both fringe signals are provided in Figs. 3(a) and 3(b). Difference in impact velocities for the shots lies within impact velocity resolution—466.7 and 462.9 m/s. Peak free-surface velocity,

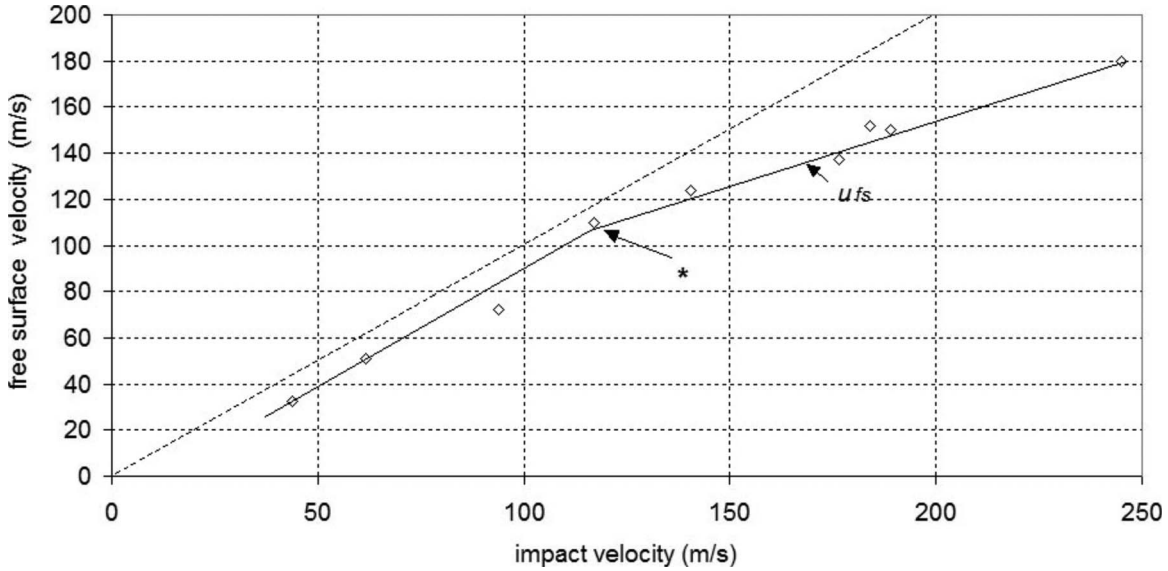

FIG. 6. Dependence of free-surface velocity on the impact velocity for a 5-mm *M*2 copper target. Instability threshold is indicated by symbol ∗.

velocity variation, and velocity deficit for both shots are also very close although they were measured under different delay shoulders of interferometer [see Figs. 3(a) and 3(b)].

The space resolution of interferometer is determined by the diameter of laser spot focused on the free surface of target ($50 \div 60$ μm).

After loading, all the specimens were cut on one of the planes along the shock direction, polished and etched using standard techniques including electropolishing. Structure study was conducted by using optical "Neophot-32" microscope and atom force microscope "nanoscan." Microhardness was measured by using "Affri" equipment with a 50-g load.

III. MESO-MACRO ENERGY EXCHANGE IN A DYNAMICALLY DEFORMED HETEROGENEOUS MEDIUM

Macroscopic response of material was registered in the form of free-surface velocity profiles. This allows us to determine the so-called "defect of free-surface velocity." ΔU is equal to the difference between peak free-surface velocity at the plateau of compressive pulse, $U_{\mathrm{fs}}^{\max}$, and independently measured impact velocity under symmetrical collision, U_{imp}:

$$\Delta U = U_{\mathrm{imp}} - U_{\mathrm{fs}}^{\max}. \tag{3.1}$$

Some comments on the defect of free-surface velocity are appropriate. There are a few of sources of the particle velocity defect. In the case of strain rate independent material, elastic plastic theory allows us to draw a dynamic stress-strain diagram only on the basis of quasistatic stress-strain diagram obtained under uniaxial stress conditions.[23,24] For the *normal stress particle velocity* variables, dynamic diagram has a configuration shown in Fig. 4. In the case of dynamic straining under uniaxial strain conditions—owing to the difference in load and release adiabatic curves—change in deformation sigh leads to double amplitude of elastic wave. Therefore, the so-called free-surface approximation $U_{\mathrm{fs}}^{\max}=2U_p$ is not true. The real release path *OABCD* does not coincide with the hypothetical symmetrical release path $OABC'D'$, which corresponds to the doubling particle velocity. As a result, the real free-surface velocity at the rear side of the target turns out to be smaller by a value of $\Delta U = U_{\mathrm{fs}}^{D} - U_{\mathrm{fs}}^{D'}$. In the shock wave literature this velocity loss is known to be the defect of free-surface velocity.[25] If elastic precursor amplitude is comparable to the plastic front amplitude, the difference between real free-surface velocities U_{fs}^{D} and doubling particle velocity $U_{\mathrm{fs}}^{D'}$ may be valuable. In the case of small value of elastic precursor, this difference is very small. For example, at the impact velocity of 400 m/s in Ti-6Al-4V titanium alloy, the elastic precursor amplitude equals $150 \div 200$ m/s—which corresponds to $2 \div 3$ GPa. Whereas for *M*3 copper it does not exceed $3 \div 5$ m/s ($0.06 \div 0.2$ GPa). In the second case, the difference between doubling particle velocity and real free-surface velocity at the rear surface of target $\Delta U = U_{\mathrm{fs}}^{D} - U_{\mathrm{fs}}^{D'}$ lies within the resolution of impactor velocity measurement ($\pm 0.5\%$) so it may be neglected.

The second source of particle velocity deficit is an interaction between elastic precursor reflected from the rear surface of target and forepart plastic front. This kind of interaction was analyzed by Grady.[26] The analysis supposes that elastic precursor is successively reflected from the free surface of target, and the plastic front gradually decreasing the latter. Owing to that interaction, both the slope of plastic front near the top of compressive pulse and peak value of particle velocity decrease. The result of simulation of that phenomenon in Ref. 27 also reveals the steplike decrease in peak value of particle velocity. It should be noted, however, that the above considerations suppose that both elastic precursor and plastic front are of wave nature, i.e., their propagation is determined by the hyperbolic type equations. In reality, elastic precursor and plastic front are known to be of

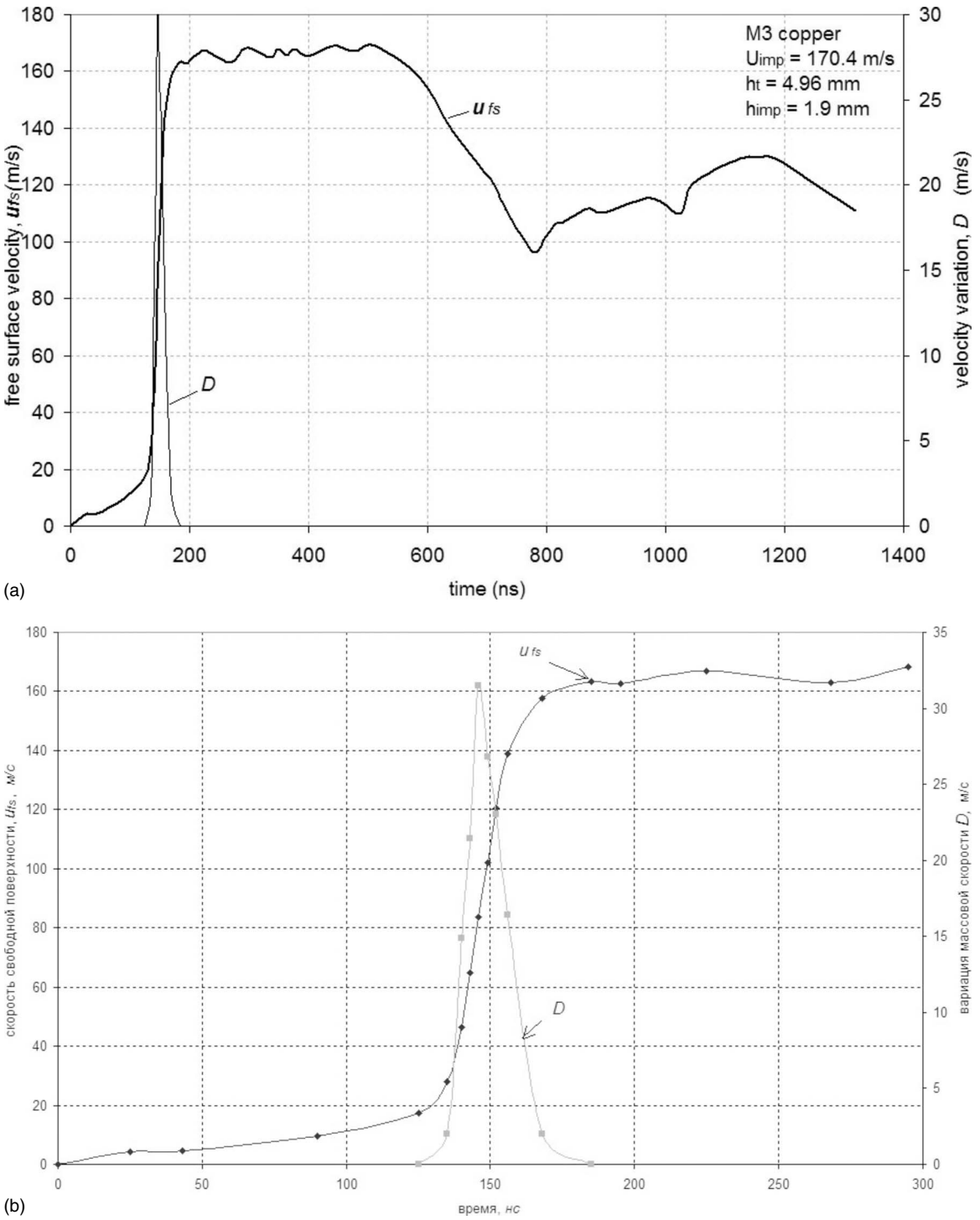

FIG. 7. Free-surface velocity, u_{fs}, and velocity variation, D, profiles for $M3$ copper target loaded at the impact velocity of 170.4 m/s: (a) common view of pulse and (b) forepart front.

relaxation nature. Thus their propagation is determined by transport processes, which are described by parabolic or mixed type equations.[28,29] This leads to extremely weak interaction of the fronts. As a result, they pass through each other without a change in their amplitudes—only small cusp at the plastic front was registered in a series of shock experiments on Armco-iron.[30,31] Besides, the effect of multiple interaction of elastic precursor and forepart plastic front turns out to be insignificant because, first, the change in the density of material at the plastic front is very small, which does not provide a hard reflection of elastic wave from plastic front. Second, under repeated reflection of elastic precursor from plastic front and free surface of target, character of interaction with the surfaces is different. During interaction with the free surface of target, the sign of particle velocity for the reflected wave changes oppositely, while during interaction with the plastic front it is conserved. Thus, during the first interaction of the elastic precursor and plastic front,

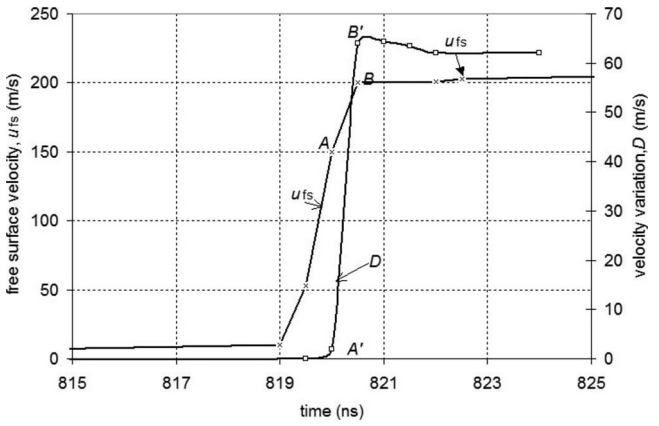

FIG. 8. Forepart front and velocity variation for the profile of Fig. 2(b) (U_{imp}=391 m/s).

amplitude of the latter decreases. Whereas during the second interaction, it increases so the resulting amplitude of plastic front does not change appreciable.

The above considerations allow us to suppose that the defect of particle velocity results from momentum and energy loss because of structural transformation occurring at the plastic front. Taylor first published a series of papers on latent energy remaining in metals after plastic deformation.[32] This is consistent with experimental measurements reviewed by Bever, Holt, and Titchener.[33] Recent experiments of Rozakis *et al.*[34] also showed that long-standing point, which is 90%–95% of plastic works, is immediately converted into heat during the dynamic straining is not true. Their experiments are based on measuring a fraction of rate of plastic work β dissipated as heat during the shock deformation. This value is inferred from the energy balance equation:

$$\rho c_v \dot{T} - kT_{xx} = \beta \sigma \dot{\varepsilon}^P - \alpha E T \dot{\varepsilon}^e, \tag{3.2}$$

where T is the temperature, and σ, ε^e, and ε^p are the longitudinal components of stress, elastic strain, and plastic strain, respectively. The material constants ρ, c_v, k, E, and v are the mass density, specific heat, thermal conductivity, thermal expansion coefficient, Young modulus, and Poisson ratio, respectively. If adiabatic conditions prevail and the rate of thermoelastic heating $\dot{Q}^e = \alpha E T \dot{\varepsilon}^e$ is negligible compared to rate of thermoplastic heating, the fraction of plastic work rate dissipated as heat is

$$\beta = \frac{\rho c_v \dot{T}}{\sigma \dot{\varepsilon}^p}. \tag{3.3}$$

In the experiments of Rozakis *et al.*, the rate of plastic work $\dot{W}^p = \sigma \dot{\varepsilon}^p$ was determined by using the Kolsky (split-Hopkinson) technique. In this technique, the strain, strain rate, and stress are measured with gauges placed on input and output bars, and specimen.[35] For *in situ* measuring the rate of thermoplastic heating, a special infrared optical system with photoconductive HgCdTe detectors was used, which provides a precise measurement of infrared radiation from deformed specimen to control the rate of thermoplastic heating.

Experiments with 2023-T3 aluminum alloy show that during the pulse loading only 30%–35% of plastic work was found to be dissipated as heat and is independent on strain rate. Above experiments cover a strain rate range between $10 \div 3 \times 10^3$ s^{-1}. For narrow shock fronts such as realized in uniaxial strain tests, the role of dissipative processes is much smaller. In this situation, energy and momentum balances in dynamically deformed medium are supported due to current energy and momentum exchange between large-scale fluctuations and macroscopic motion of medium. Herewith, the large-scale velocity fluctuations must not be identified with the thermodynamical temperature. For highly nonequilibrium processes the concept of temperature is known to be incorrect. The particle velocity dispersion generalizes the concept of temperature on nonequilibrium processes when thermodynamical temperature loses its physical meaning. As distinct from the thermal fluctuations, mesoscale fluctuations are not complied with the second thermodynamics law. For the finite time interval, in particular, during the rise time of steady plastic wave front, energy, and momentum exchange between mean particle velocity and mesoscale fluctuations may be reversible, similar to exchange between large-scale pulsations and average flow velocity in turbulence phenomenon for liquid.[36] At that stage, the particle velocity fluctuations may cause the effects of self-organizing, i.e., formation of mesoscale structures. In the long-time limit, owing to relaxation processes, transition from large-scale fluctuations to irreversible chaotic fluctuations at the atom scale occurs, i.e., relaxation process transits into dissipative stage. In the west literature, the intensity of large-scale particle velocity fluctuations often calls a "granular temperature." In material science, the term "large scale" means that the space dimensions of structure elements belong to the so-called mesoscale (typical dimension $l_{meso} = 10^{-5} \div 10^{-3}$ cm) occupying intermediate position between microscale ($l_{micro} = 10^{-7} \div 10^{-6}$ cm) and macroscale ($l_{macro} = 10^{-1} \div 10^{-3}$ cm).

In the case of nonequilibrium processes in solids, the "equation of state (EOS)" problem and constitutive equation for material are the key problems. In our approach, the propagation of shock wave in heterogeneous medium is considered to be a stochastic process, which is described in terms of nonequilibrium particle velocity distribution function, $f(r,v,t)$.[37] The plastic particle velocity, u^{pl}, is subdivided in equilibrium and nonequilibrium parts:

$$u^{pl} = u^{pl}_{eq} + u^{pl}_{ne.} \tag{3.4}$$

Herewith, equilibrium part of plastic particle velocity, u^{pl}_{eq}, and nonequilibrium part of particle velocity, u^{pl}_{ne}, are determined by the equilibrium, f_0, and nonequilibrium, f_1, parts of the particle velocity distribution function, respectively, as the first statistical moments of the particle velocity distribution function:

$$u^{pl}_p = \frac{1}{\rho}\int_{-\infty}^{\infty} u f_0 du, \quad u^{pl}_{\pi} = \frac{1}{\rho}\int_{-\infty}^{\infty} u f_1 du, \tag{3.5}$$

where

$$f = f_0 + f_1.$$

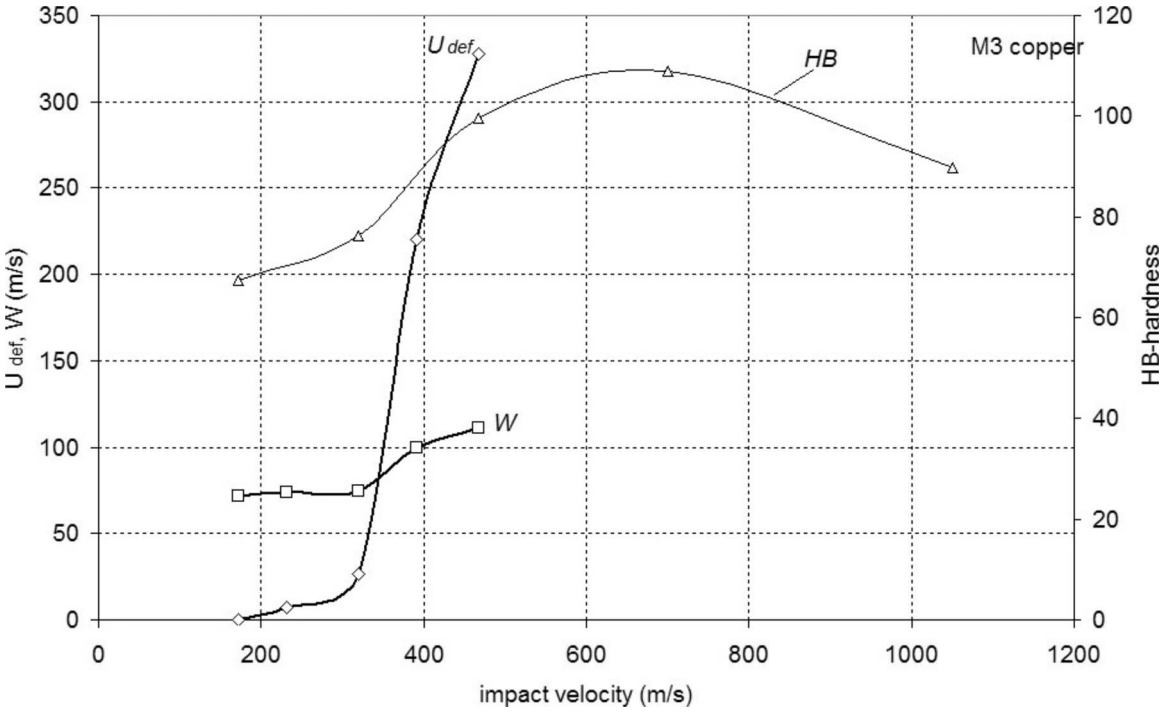

FIG. 9. Defect of free-surface velocity ΔU, pull back velocity W, and HB hardness versus impact velocity.

Total stress σ^m is also consists of equilibrium and nonequilibrium parts,

$$\sigma^m = \sigma^m_{\text{eq}} + \sigma^m_{\text{ne}}, \tag{3.6}$$

where the equilibrium part σ^m_{eq} characterizes the stress value at the Hugoniot adiabate,

$$\sigma^m_{\text{eq}} = \rho C_l u^{\text{pl}}_{\text{eq}}. \tag{3.7}$$

Physically, the first component of stress in Eq. (3.6), σ^m_{eq}, results from thermal fluctuation and is defined by EOS for concrete material. The second component, σ^m_{ne}, is determined by large-scale fluctuations of medium. The quantitative characteristic of large-scale fluctuations is the particle velocity dispersion, which is the second statistical moment of the particle velocity distribution function $f(v)$:

$$D^2 = M(v-u)^2 = \int_{-\infty}^{\infty} (v-u)^2 f(v) dv. \tag{3.8}$$

The nonequilibrium stress includes a spherical component P^m and deviator, S:

$$\sigma^m_{\text{ne}} = P^m - S. \tag{3.9}$$

In the present consideration, we want to account for only an effect of particle velocity dispersion on wave propagation in heterogeneous medium. It is accepted that deviator item does not contribute into momentum transportation, i.e., $S=0$. With due regard for mesoscale effects, P^m is an addition due to large-scale velocity fluctuations at the mesoscale. Mesoscale pressure P^m can be written through the mesoparticle velocity variation, D, in the form:

$$P^m = \rho D^2, \tag{3.10}$$

At dissipative stage of relaxation process, the mesoscale pressure transits into thermal pressure:

$$\sigma^m_{\text{ne}} = \rho D^2 \to 3NkT. \tag{3.11}$$

In this situation, the first question that arises is what kind of nonlinearity lays in that approach. As noticed, the large-scale fluctuations at the mesoscale provide an addition to spherical component of pressure in a medium. As distinct from the yielding value, which characterizes a plastic threshold of material, the rate of change in particle velocity dispersion characterizes a strain rate nonlinearity of redistribution of dilatation between macroscopic and mesoscopic components. Change in the particle velocity dispersion nonlinearly influences on the mean motion of assemble of particles. When the velocity dispersion increases, the common motion of assemble slows down, and vice versa, with the decrease in the particle velocity dispersion the mean velocity of assemble increases. The reason for such behavior of heterogeneous medium and appearance of the mean velocity defect lies in negative back coupling between first statistical moment of the particle velocity distribution function (mathematical expectation) and second statistical moment (velocity dispersion). This coupling results from cumulative action of long-range interaction between mesoparticles, boundary conditions, and external load. Mathematically, the coupling between velocity defect, Δu, and mesoparticle velocity dispersion, D^2, is written in the form:[38]

$$\Delta u = -\frac{1}{2}\frac{dD^2}{du}. \tag{3.12}$$

This equation was experimentally verified to be hold for large variety of materials including aluminum and aluminum

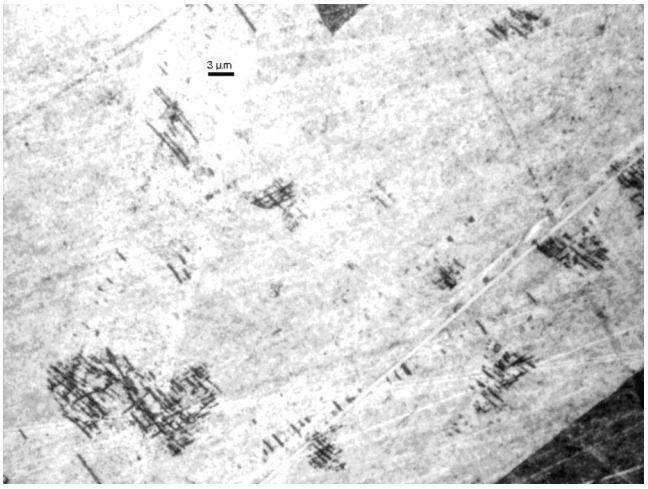

FIG. 10. Solitary centers of vortical structure at the impact velocity of 391 m/s (shock direction—from top to bottom).

alloys, steels, titanium alloys, beryllium, and copper. Using a definition of strain rate under uniaxial strain conditions $\dot{\varepsilon} = u/C_0$, Eq. (3.12) may be written as follows:

$$\frac{\Delta u}{C_0} = -\frac{1}{2}\frac{dD^2}{du} = -\frac{D}{C_0}\frac{dD}{du} = -\frac{D}{C_0}\frac{\frac{dD}{dt}}{\frac{du}{dt}} = -\frac{D}{C_0}\frac{\frac{1}{C_0}\frac{dD}{du}}{\frac{1}{C_0}\frac{du}{dt}}$$

$$= -\varepsilon_D \frac{\dot{\varepsilon}_D}{\dot{\varepsilon}_u}. \tag{3.13}$$

Here C_0 is the shock wave velocity, $\Delta\varepsilon = \Delta u/C_0$ is an addition to macrodeformation due to meso-macro energy and momentum exchange, $\varepsilon_D = D/C_0$ is a mesoscale deformation—i.e., localized deformation at the mesoscale due to particle velocity distribution—and $\varepsilon_u = u/C_0$ is the macrodeformation. When the strain rate at the mesoscale is equal to the rate of macrodeformation,

$$\dot{\varepsilon}_D = \dot{\varepsilon}_u, \tag{3.14}$$

the addition to macrodeformation is exactly equal to the deformation at the mesoscale:

$$\Delta\varepsilon = \varepsilon_D. \tag{3.15}$$

In this case, defect of particle velocity equals the velocity variation:

$$\Delta u = D. \tag{3.16}$$

One of the advantages of Eq. (3.16) is that both sides of the equation can be registered independently during the shock tests. Equations (3.15) and (3.16) reflect a balance regime of meso-macro momentum exchange, which corresponds to steady wave processes. In this case, according to experiments, the material has a maximum dynamic plasticity and strength, including spall strength. Several examples of such a kind of behavior of steels are provided in Ref. 37.

If strain rate at the mesoscale is much higher than macroscopic strain rate, i.e.,

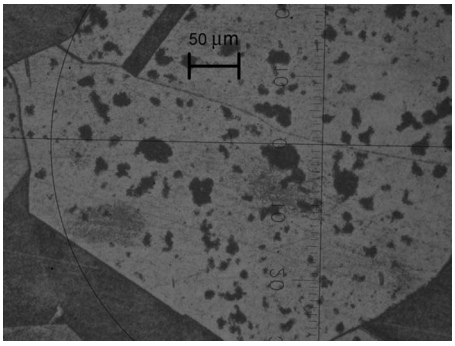

FIG. 11. Solitary centers of vortical structure at the impact velocity of 466.7 m/s

$$\dot{\varepsilon}_D \gg \dot{\varepsilon}_u, \tag{3.17}$$

heterogeneity of material reveals in the form of shear banding.[37] In opposite case, when

$$\dot{\varepsilon}_D \ll \dot{\varepsilon}_u, \tag{3.18}$$

mesostructure has no time to accommodate the external load, which leads to the increase in internal stresses and the decrease in dynamic strength.

Equation (3.12) determines a current value of the mean particle velocity change. To obtain the mean particle velocity loss due to meso-macro momentum exchange over the shock front ΔU, Eq. (3.12) must be integrated over the plastic front duration, τ_f:

$$\Delta U = \int_0^{\tau_f} \Delta u dt. \tag{3.19}$$

Experiments show that for steady front the summary velocity defect at the top of front is equal to zero ($\Delta U = 0$). This means that for steady wave the strain behavior of material is nonlinear but reversible. Qualitatively, the process of meso-macro momentum exchange for the steady plastic front is presented in Fig. 5(a). In this figure, for simplicity, the position of shock front in the absence of meso-macro momentum exchange is shown in the form of straight line *OLN*. In the presence of momentum exchange, during the first half of shock front, a transmission of momentum from macroscale to mesoscale takes place. Herewith, growth of mean particle velocity slows down while the velocity variation increases. During the second part of front, the reverse process flows—momentum of mesoscale fluctuations is transferred on to macroscale.

For unsteady shock front irreversible transmission of momentum from macroscale to mesoscale flows along whole front resulting in decrease in mean particle velocity at the top of front and appearance of defect of mean particle velocity ($\Delta U \neq 0$). Qualitative picture of such meso-macro momentum exchange is provided in Fig. 5(b). This situation corresponds to irreversible nonlinear response of material on shock loading. One of the examples of threshold behavior of the particle velocity defect is provided in Fig. 6 where a dependence of free-surface velocity on the impact velocity is plotted. One can see that up to the impact velocity of 130 m/s

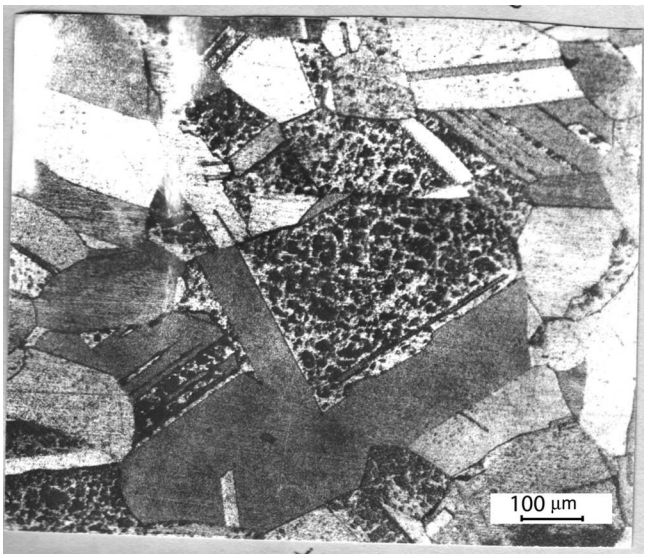

FIG. 12. Turbulentlike structures at the impact velocity of 650 m/s.

the dependence $U_{\rm fs}=f(U_{\rm imp})$ is parallel to the diagonal $U_{\rm fs}=U_{\rm imp}$, corresponding to "free-surface approximation." After the impact velocity of 130 m/s, the slope of dependence $U_{\rm fs}=f(U_{\rm imp})$ decreases, which means that velocity defect increases. Similar dependencies have been found for several kinds of metals such as constructional steels, beryllium, aluminum alloys, titanium alloys, and others.

IV. CRITERION FOR SHOCK INDUCED STRUCTURAL TRANSITION

Shock tests of a variety of materials reveal two regimes of energy exchange between mesoscale and macroscale—homogeneous and "catastrophic" regimes. The latter supposes that mean particle velocity at the plastic front of compressive pulse at some strain rate stops to grow while the particle velocity dispersion increases. The irreversible growth of the particle velocity defect is directly related to transition from homogeneous to catastrophic regime of micro-macro energy exchange.

Let us consider a propagation of plane one-dimensional wave in a medium. Without accounting for thermoconductivity processes, motion of medium is described by two balance equations:

$$\rho\frac{\partial u}{\partial t}=\frac{\partial \sigma}{\partial x}, \tag{4.1}$$

$$\frac{\partial u}{\partial x}=\frac{\partial \varepsilon}{\partial t}. \tag{4.2}$$

Here $\partial\varepsilon/\partial t$ is a total (elastic plus plastic) strain rate in the wave propagation direction. It may be decomposed in the form,

$$\frac{\partial \varepsilon}{\partial t}=\frac{\partial \varepsilon^e}{\partial t}+\frac{\partial u^{pl}}{\partial x}. \tag{4.3}$$

Similar representation is known to be held in continuum theory of dislocations where the last item is expressed through dislocation velocity tensor.[39] Then the continuity equation becomes:

$$\frac{\partial u}{\partial x}=\frac{\partial \varepsilon^e}{\partial t}+\frac{\partial u^{pl}}{\partial x}. \tag{4.4}$$

Here $\partial\varepsilon^e/\partial t$ is an elastic strain rate and $\partial u^{pl}/\partial x$ is a plastic strain rate, respectively. Normal stress may also be presented as sum of elastic and nonelastic components:

$$\sigma=\sigma^e+\sigma^m, \tag{4.5}$$

where elastic component of stress is determined by the Hook law:

$$\sigma^e=(\lambda+2\mu)\varepsilon^e, \tag{4.6}$$

The meaning of nonelastic component σ^m was given in the previous section. Taking into account Eqs. (4.3) and (4.4), the balance equations for mass and momentum can be reduced to the second-order equation:

$$\frac{\partial^2 u}{\partial x^2}-\frac{1}{c_l^2}\frac{\partial^2 u}{\partial t^2}=\frac{\partial^2 u^{\rm pl}}{\partial x^2}-\frac{1}{(\lambda+2\mu)}\frac{\partial^2 \sigma^m}{\partial x\,\partial t}, \tag{4.7}$$

where $c_l=[(\lambda+2\mu)/\rho]^{1/2}$ is a longitudinal sound velocity and the left side of the equation is a wave operator for the total particle velocity in a medium.

Equilibrium part of the particle velocity distribution function is a Maxwell distribution. To determine a nonequilibrium part of distribution function, f_1, kinetic equation of relaxation kind can be used:[40]

$$\frac{\partial f}{\partial t}+u\frac{\partial f}{\partial r}+\langle \dot{u}\rangle\frac{\partial f}{\partial u}=-\frac{f-f_0}{\tau_r}, \tag{4.8}$$

where τ_R is a relaxation time for particle velocity distribution function. In dynamically deformed solids, relaxation time at the mesoscale is very small. Specifically, simulation of dynamic processes for copper gives for relaxation time a value of $\tau_R=11.5$ ns.[12] This means that the change in particle velocity distribution function due to relaxation processes flows much faster than on account for convective mass transportation. Thus the first two items in the left-hand side of Eq. (4.8) may be neglected. Then,

$$f_1=-\tau_R\langle \dot{u}\rangle\frac{\partial f_0}{\partial u}. \tag{4.9}$$

In common case, mean acceleration $\langle \dot{u}\rangle$ must be determined from interaction potential, Π, as $\langle \dot{u}\rangle=1/m\,\mathrm{grad}\ \Pi$. However, interaction potential for mesoparticles is not determined once and for all. According to modern representations of physics of plasticity,[41] mesostructure is a highly nonuniform polarized dislocation structure with space separation of dislocation groups in sign (see Sec. VI). Long-range interaction

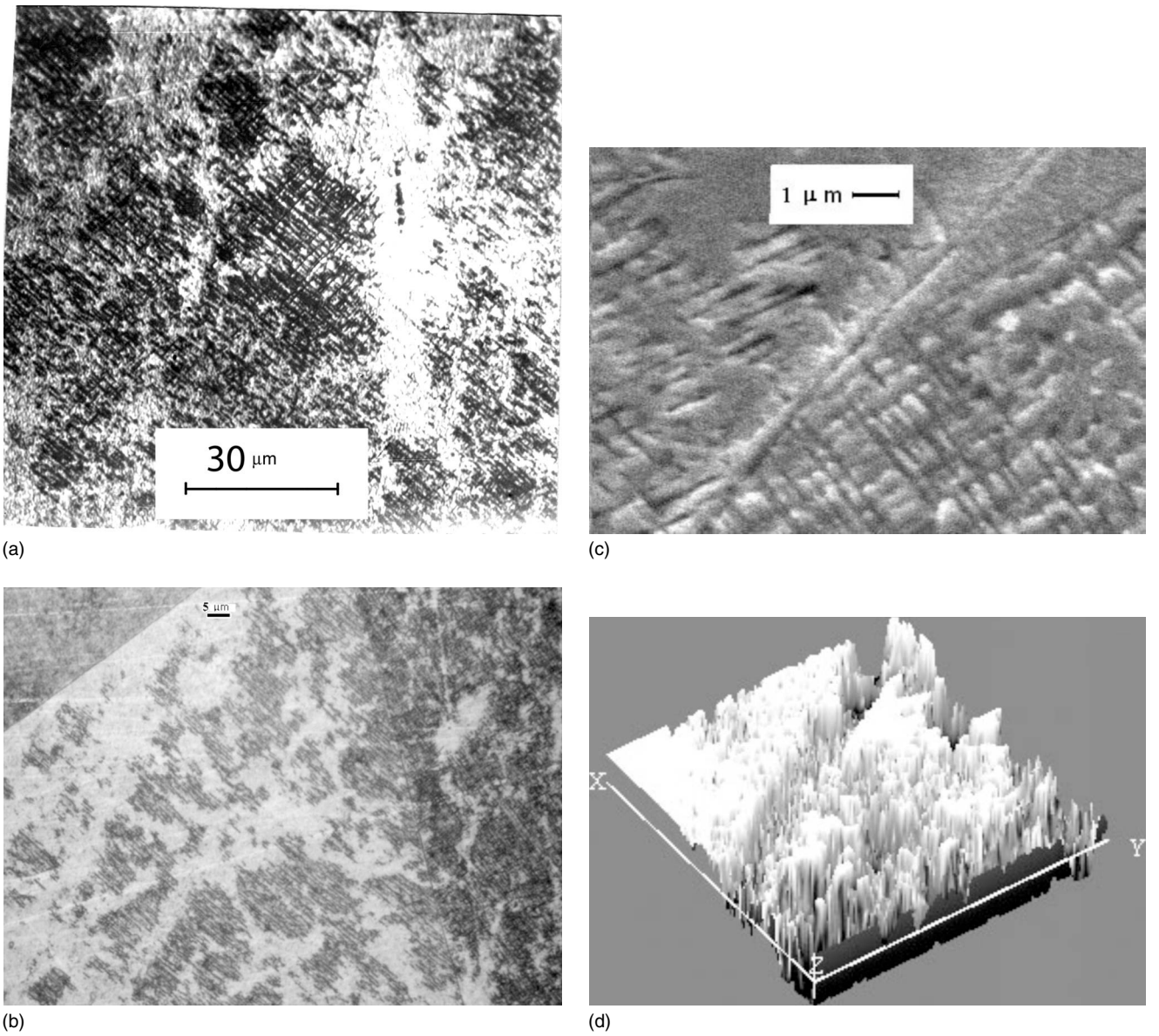

FIG. 13. Interior of vortical cell: (a) optical microscopy, (b) optical microscopy of two neighbor grains with structured and clear interior, (c) atom force microscopy, and (d) three-dimensional view of neighbor grains.

between dislocations permits to build the so-called electromagnetic analogy.[42,43] In a sense, dislocation structure closely reminds the continuum of charged particles although the character of interaction of dislocation groups is not central and the azimuth component of interaction may be valuable. For determination of mean acceleration $\langle \dot{u} \rangle$, we make use of the fact of similarity between dislocation structure and continuum of charged particles. In this case, the mean acceleration of mesoparticle has the same meaning as the first diffusive coefficient in the Fokker-Plank equation, which is commonly used for description of nonequilibrium processes in stochastic media:[44]

$$F_1 = \frac{\langle \Delta u \rangle}{\Delta t}, \tag{4.10}$$

where $\langle \Delta u \rangle$ is the average change in particle velocity, which is much greater than the individual velocity fluctuation in a stochastic medium but much smaller than the macroscopic change in particle velocity in shock wave process. The right-hand side of Eq. (4.10) has a meaning of acceleration and is being multiplied by mass of mesoparticle, equals the so-called drift force. For the fluctuating medium of charged particles Hubburd[44] found the following relationship between first and second diffusive coefficients of the Fokker-Plank equation:

$$F_1 = -\frac{1}{2}\frac{dF_2}{du}. \tag{4.11}$$

Here F_2 is the second diffusion coefficient in the velocity space,

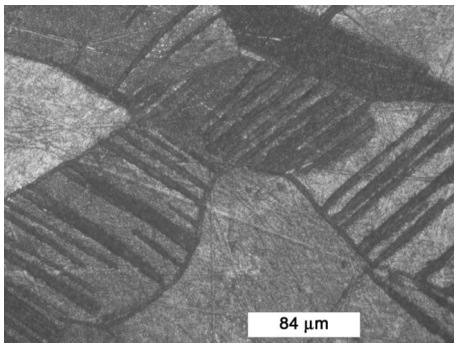

FIG. 14. Cross section of target with twins at the impact velocity of 1050 m/s (shock direction—from top to bottom).

$$F_2 = \frac{\langle \Delta u \Delta u \rangle}{\Delta t}, \tag{4.12}$$

which is determined through the particle velocity dispersion $D^2 = \langle \Delta u \Delta u \rangle$ as

$$F_2 = \frac{D^2}{\Delta t}. \tag{4.13}$$

Equation (4.10) can be rewritten as follows:

$$F_1 \frac{\langle \Delta u \rangle}{\Delta t} = -\frac{1}{2}\frac{1}{\Delta t}\frac{dD^2}{du}. \tag{4.14}$$

It also can be written in the form,

$$\Delta u = -\frac{1}{2}\frac{dD^2}{du}, \tag{4.15}$$

which exactly coincides with Eq. (3.12) obtained on the basis of experiments. It may be concluded that Eq. (3.12), similar to Eq. (4.15), also reflects the coupling between first statistical moment of the particle velocity distribution function (mathematical expectation) and second statistical moment (particle velocity dispersion).

Taking into account that the mean change in particle velocity, $\langle \Delta u \rangle$, occurs for the relaxation time $\Delta t = \tau_R$, one obtains

$$\langle \dot{u} \rangle = \frac{\langle \Delta u \rangle}{\tau_R} = -\frac{1}{2}\frac{1}{\tau_R}\frac{dD^2}{du}. \tag{4.16}$$

Then, the nonequilibrium part of the particle velocity distribution function is

$$f_1 = -\frac{1}{2}\frac{\partial f_0}{\partial u}\frac{\partial D^2}{\partial u}, \tag{4.17}$$

and for nonequilibrium part of particle velocity, one obtains

$$u_{\mathrm{ne}}^{\mathrm{pl}} = \frac{1}{\rho}\int_{-\infty}^{\infty} u f_1 du = -\frac{1}{2}\frac{\partial D^2}{\partial u}. \tag{4.18}$$

Thus, Eq. (4.18) asserts that the nonequilibrium part of plastic particle velocity is exactly equal to the particle velocity defect. Substitution of Eqs. (3.9), (3.10), and (4.18) into Eq. (4.7) gives

$$C_0^2\left[1 - \left(\frac{D}{u}\frac{\partial D}{\partial u}\right)\right]\frac{\partial^2 u}{\partial x^2} - \frac{\partial^2 u}{\partial t^2} = C_0^2\frac{\partial^2 u_{\mathrm{eq}}^{\mathrm{pl}}}{\partial x^2} + \frac{1}{2}C_0^2\frac{\partial^2}{\partial x^2}\frac{\partial D^2}{\partial u} - \frac{\partial^2}{\partial x\,\partial t}(C_0 u_{\mathrm{eq}}^{\mathrm{pl}}) - \frac{\partial}{\partial t}\left(\frac{\partial D^2}{\partial x}\right). \tag{4.19}$$

The first and the third items in right-hand side, which concern the equilibrium part of momentum transportation, annihilate because at the Hugoniot adiabate the process is steady. In other words, equilibrium components of plastic particle velocity, $u_{\mathrm{eq}}^{\mathrm{pl}}$, do not contribute in the change in total velocity profile. Then Eq. (4.19) can be written as follows:

$$C_0^2\frac{\partial^2 u}{\partial x^2} - \frac{\partial^2 u}{\partial t^2} = \frac{1}{2}C_0^2\frac{\partial^2}{\partial x^2}\left(\frac{\partial D^2}{\partial u}\right) - \frac{\partial}{\partial t}\left(\frac{\partial D^2}{\partial x}\right). \tag{4.20}$$

Derivatives in the right-hand side of the equation may be presented in the form:

$$\frac{\partial}{\partial t}\left(\frac{\partial D^2}{\partial x}\right) = 2\frac{\partial}{\partial t}\left(u \cdot \frac{D}{u}\frac{\partial D}{\partial x}\right) = 2\frac{\partial u}{\partial t}\left(\frac{D}{u}\frac{\partial D}{\partial x}\right) + 2u\frac{\partial}{\partial t}\left(\frac{D}{u}\frac{\partial D}{\partial x}\right), \tag{4.21}$$

$$2\frac{\partial u}{\partial x}\left(\frac{D}{u}\frac{\partial D}{\partial u}\right) + 2u\frac{\partial}{\partial t}\left(\frac{D}{u}\frac{\partial D}{\partial x}\right), \tag{4.22}$$

$$\frac{\partial^2}{\partial x^2}\left(\frac{\partial D^2}{\partial u}\right) = 2\frac{\partial^2}{\partial x^2}\left(u \cdot \frac{D}{u}\frac{\partial D}{\partial u}\right) + 4\frac{\partial}{\partial x}\left(\frac{D}{u}\frac{\partial D}{\partial u}\right) + 2u\frac{\partial}{\partial t}\left(\frac{D}{u}\frac{\partial D}{\partial u}\right) + 2u\frac{\partial^2}{\partial x^2}\left(\frac{D}{u}\frac{\partial D}{\partial u}\right). \tag{4.23}$$

Substitution of Eqs. (3.4), (3.5), (4.17), and (4.21)–(4.23) into Eq. (4.7) gives

$$C_0^2\left[1 - \left(\frac{D}{u}\frac{\partial D}{\partial u}\right)\right]\frac{\partial^2 u}{\partial x^2} - \frac{\partial^2 u}{\partial t^2} = 2\frac{\partial^2}{\partial x^2}\left(u \cdot \frac{D}{u}\frac{\partial D}{\partial u}\right) + 4\frac{\partial}{\partial x}\left(\frac{D}{u}\frac{\partial D}{\partial u}\right) + 2u\frac{\partial}{\partial t}\left(\frac{D}{u}\frac{\partial D}{\partial u}\right) + 2u\frac{\partial^2}{\partial x^2}\left(\frac{D}{u}\frac{\partial D}{\partial u}\right) - 2\frac{\partial u}{\partial x}\left(\frac{D}{u}\frac{\partial D}{\partial u}\right) - 2u\frac{\partial}{\partial t}\left(\frac{D}{u}\frac{\partial D}{\partial x}\right). \tag{4.24}$$

One can see that when

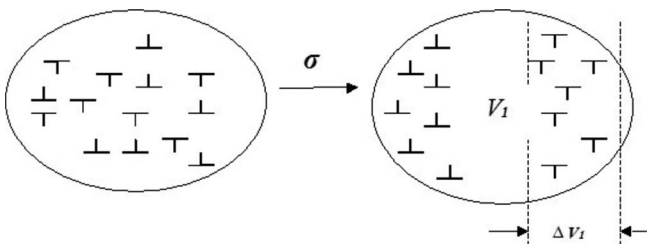

FIG. 15. Scheme of polarized dislocation structure.

TABLE I. Macroscopic response of M3 copper on impact.

Impact velocity (m/s) ±0.5%	170.4	231.9	319.6	391	466.7	500	1050
Velocity defect (m/s) ±0.5%	0	7.4	24.6	172.6	364		
Pull back velocity (m/s) ±0.3%	72	73.7	105	105.4	111		
HB hardness ±4%	67.5	73.6	76.3	90.5	94.5	109	89.7

$$\left(\frac{D}{u}\frac{\partial D}{\partial u}\right) = 1, \tag{4.25}$$

Eq. (4.24) is reduced to equation

$$\frac{\partial^2 u}{\partial t^2} = -2u\frac{\partial u}{\partial t}\left(\frac{D}{u}\frac{\partial D}{\partial x}\right) - 2\frac{\partial u}{\partial t}\left(\frac{D}{u}\frac{\partial D}{\partial x}\right). \tag{4.26}$$

By using Eq. (4.25), $[(D/u)(\partial D/\partial x)]$ can be transformed as follows:

$$\left(\frac{D}{u}\frac{\partial D}{\partial x}\right) = \frac{\partial u}{\partial x}. \tag{4.27}$$

Then Eq. (4.26) takes the form,

$$\frac{\partial^2 u}{\partial t^2} + 2u\frac{\partial u}{\partial t}\frac{\partial u}{\partial x} + 2\frac{\partial u}{\partial t}\frac{\partial u}{\partial x} = 0. \tag{4.28}$$

This nonlinear equation is not analyzed in this paper. Note only that it describes the highly decaying processes. Equation (4.25) may be transformed as follows:

$$\left(\frac{D}{u}\frac{\partial D}{\partial u}\right) = \left(\frac{D}{u}\frac{\dot{D}}{\dot{u}}\right) = 1. \tag{4.29}$$

When condition Eq. (4.29) is fulfilled, the wave motion of medium is transformed into the decaying of particle velocity. It is seen that catastrophic loss of particle velocity at the plastic front is determined both by ratio of dispersion and mean velocity and by ratio of rates of their changing (accelerations). In case of shock-deformed solid, the above characteristics are measurable dynamic values.[21,22]

Criterion Eq. (4.29) can be applied to concrete particle velocity profiles for copper. In Figs. 7(a) and 7(b) the steady free-surface velocity profile, u_{fs}, and velocity variation profile, D, for the $M3$ copper target loaded at the impact velocity of 170.4 m/s are provided. Handling the profiles gives

$$\frac{D}{u} = 0.377, \quad \frac{\dot{D}}{\dot{u}} = 0.531 \quad \text{and} \quad \frac{D}{u}\frac{\dot{D}}{\dot{u}} = 0.2.$$

Thus the criterion Eq. (4.29) is not fulfilled.

The same procedure for the unsteady profiles of Figs. 2(b) and 8 at the impact velocity of 391 m/s (pieces AB and $A'B'$ of the velocity profile) gives

$$\frac{D}{u} = 0.842, \quad \frac{\dot{D}}{\dot{u}} = 1.24 \quad \text{and} \quad \frac{D}{u}\frac{\dot{D}}{\dot{u}} = 1.04.$$

Thus the criterion Eq. (4.29) is fulfilled and the mean particle velocity suffers a break at position B.

V. MACROSCOPIC RESPONSE OF MATERIAL ON SHOCK LOADING

Parameters of loading and results of tests are provided in Table I. Besides the defect of particle velocity, additional macroscopic characteristics controlled in our tests are the pull back velocity W, which characterizes a spall strength of material, and the HB hardness measured with a standard technique. Dependencies of the free-surface velocity defect, pull back velocity, and HB hardness on impact velocity are presented in Fig. 9. Up to impact velocity of 170.4 m/s, defect of the free-surface velocity is equal to zero. A valuable growth of the particle velocity defect occurs when impact velocity increases from 391 to 466.7 m/s, which correlates with the spall strength and hardness behavior.

VI. MICROSTRUCTURE INVESTIGATIONS

It is interesting to compare the behavior of macroscopic characteristics of material response on shock loading and the peculiarities of structure formation for different strain rates. Up to impact velocity of 319 m/s, a change in defect structure of copper, as compared to initial state, is not found. The first solitary centers of nucleation of vortical structures were found at the impact velocity of 391 m/s. These centers look like solitary spots consisting of networks of mutual perpendicular twins of 100–300 nm spacing. Typical pattern of this kind of structures is provided in Fig. 10. With the increase in strain rate, density of the network centers increases (Fig. 11). The increase continues up to impact velocity of 500 m/s. After that dimension of spots begins to grow whereas their density remains invariable. A typical picture of turbulent structure at the impact velocity of 650 m/s is shown in Fig. 12, where it is observed that the turbulentlike structures lie in the grains favorable oriented with respect to shock direction. The interiors of grains are filled with the formations of $5 \div 25$ μm in diameters. Under increased magnification each dark spot looks like network of microshear bands of 0.2–0.3 μm spacing [Figs. 13(a)–13(d)]. At high strain rates of $10^7 \div 10^9$ s^{-1}, the basic mechanism of structural heterogenization of copper is known to be the twinning.[9] The critical twinning pressure equals 20 GPa for [111] direction,[45] which corresponds to impact velocity of ~1000 m/s. Increase in impact velocity to 1050 m/s leads to the disappearance of the turbulentlike structures giving the place for twins (Fig. 14).

The grains with microband structures have higher microhardness than that for "clear" grains: 1440 ± 80 and 1210 ± 40 N/mm^2, respectively.

VII. DISCUSSION

Macroscopic response and microstructure data presented in Secs. IV and V showed that both nucleation of dissipative structures and nonmonotonous behavior of dynamic strength of material have typical features of resonance phenomenon. The resonance condition is thought to be established between periodical density of dislocation charge and space dimension of plastic front. As mentioned in Sec. V, physics of plasticity considers the mesoscale formation as a collective dislocation phenomenon resulted in polarization of dislocation structure. Basic feature of mesoscale is that in its specific volumes, under action of stress field, the initially uniform and quasineutral distribution of dislocations re-forms into highly nonuniform dislocation distribution with polarization of different in sigh dislocations—the so-called heterogeneity of dislocation ensemble (see Fig. 15). For the majority of real situations, macroscopic plastic deformation is basically determined by the processes flowing at the mesoscale. The total spectrum of the most essential for the macroscopic behavior rearrangements of dislocation ensemble including the evolution of the latter from ball to fragmented structures, shear banding, and rotational plasticity are realized at the scales $l_1 \approx (0.1 \div 10)\mu$m.[42] The mesovolume with polarized dislocation ensemble is considered to be a quasiparticle with effective charge of $\Delta q \approx \Delta\rho\Delta V_1$ so it has a much larger interaction radius compared to quasineutral state. In a sense, the mesostructure is similar to the continuum of charged particles, which justifies the electromagnetic analogy. The mean size of mesoparticle is determined by the free run distance of dislocations under driving force,

$$l_1 = v_d \cdot \tau_p, \tag{7.1}$$

where v_d is a dislocation velocity and τ_p is a duration of driving stress pulse.

In the case of uniaxial straining, formation of mesostructure is shown to be initiated elsewhere at the elastic precursor of plane elastic plastic wave.[13] The rise time of which for copper ranges from 50 ns for impact velocity of 170.4 m/s to 5 ns for impact velocity of 466.6 m/s. As for the dislocation velocity, for our estimates its value may be taken to be a transverse sound speed in copper $v_\perp = 2.26 \times 10^5$ cm/s. Then the mean run of dislocations equals 11.3 μm and space period of polarized structure equals $l_1 = 22.6$ μm, which coincides with the mean dimension of dynamic structures. The formed structure at the elastic precursor periodical polarized dislocation structure interacts with the following plastic front, rise time of which is also approximately 5.5 ns for the impact velocity of 466.7 m/s. Plastic front speed in copper approximately equals 3.9 mm/μs so the space dimension of plastic front is equal to $l_{\mathrm{pl}} = C_{\mathrm{pl}} \cdot \tau_f = 3.9 \times 10^5 (\mathrm{cm/s}) \cdot 5.5 \times 10^{-9} (\mathrm{s}) = 21.5$ μm, which is within the mean dimension of separate cell of "frozen" dynamic structure. The resonance interaction of plastic front and periodical polarized dislocation structure leads to the swinging of the large-scale particle velocity fluctuations and to particle velocity variation. As distinct from the mean particle velocity for the uniaxial strain conditions, velocity variation at the mesoscale is a three-dimensional value—which results in nucleation of rotational structures, dimensions of which coincide with the period of polarized dislocation.

Resonance coincidence of plastic front width and period of polarized dislocation structure is necessary but not a sufficient condition for nucleation of dissipative structures. In a solid with a crystalline structure, shearing and rotation may be realized only along the proper crystalline planes and directions. Specifically, in copper these are {100} planes and [111] directions. For the proper sliding to be initiated, the value of Schmidt factor must be provided by the appropriate orientation of grains, relatively shock wave direction. This is clearly seen in Figs. 12 and 13 where nucleation of dissipative structures depends on orientation of grains.

VIII. CONCLUSIONS

Conclusive evidence drawn from investigation was that the shock induced turbulentlike structures in copper are nucleated within range of impact velocities from ~400 to ~650 m/s. They have a microshear band morphology resulted from crystalline nature of plastic deformation. Nucleation of dissipative structures occurs under simultaneous action of high pressure provided by uniaxial straining and shear along the crystalline planes. Physical mechanism for nucleation of dissipative structures is thought to be a resonance interaction between polarized periodical dislocation structure (mesostructure) and space period of driving elastic plastic wave. Under resonance condition, particle velocity variation begins to grow faster than mean particle velocity. Simultaneously, defect of particle velocity at the plateau of compressive pulse, macrohardness, and spall strength grow in the same manner.

Increase in macroscopic strength of material, both spall strength (1.55 times) and macrohardness (1.4 times), may be attributed to partitioning the favorably oriented grains.

ACKNOWLEDGMENTS

This work was supported by the Russian Foundation for Basic Research Projects No. 08-02-0329 and No. 08-02-004. We would like to thank S. V. Rasorenov for checking the results in his own experimental configuration.

*Present address: Central Research Institute of Constructional Materials "Prometey," Saint Petersburg, Russia.

[1] L. E. Murr, in *Shock Waves and High-Strain-Rate Phenomena in Metals*, edited by M. A. Meyers and L. E. Murr (Plenum, New York, 1981), pp. 607–673.

[2] M. A. Meyers and L. E. Murr, in *Shock Waves and High-Strain-Rate Phenomena in Metals*, edited by M. A. Meyers and L. E. Murr (Plenum, New York, 1981), pp. 121–151.

[3] J. R. Asay and L. C. Chhabildas, in *Shock Waves and High-Strain Phenomena in Metals*, edited by M. A. Meyers and L. E. Murr (Plenum, New York, 1981), p. 417.
[4] D. E. Grady and M. E. Kipp, J. Mech. Phys. Solids **35**, 95 (1987).
[5] G. T. Gray III, in *High-Pressure Shock Compression of Solids VI*, edited by J. R. Asay and M. Shahinpoor (Springer-Verlag, New York, 1993), pp. 187–215.
[6] Y. Bai and B. Dodd, *Adiabatic Shear Localization* (Plenum, Oxford, 1992).
[7] M. A. Meyers, *Dynamic Behavior of Materials* (Wiley, New York, 1994).
[8] R. W. Armstrong, C. S. Coffey, and W. L. Bilban, Acta Metall. **30**, 2111 (1982).
[9] L. E. Murr and E. V. Esquivel, J. Mater. Sci. **39**, 1153 (2004).
[10] Yu. I. Mescheryakov, A. N. Makhutov, and S. A. Atroshenko, J. Mech. Phys. Solids **42**, 1435 (1994).
[11] J. Lee, in *High-Pressure Shock Compression of Solids VI*, edited by Lee Davison and Yashi-Yuki Horie (Springer-Verlag, Berlin, 2002), pp. 122–148.
[12] K. Yano, and Y. Horie, Phys. Rev. B **59**, 13672 (1999).
[13] M. Yu. Gutkin, I. A. Ovid'ko, and Yu. I. Mescheryakov, J. Phys. III **3**, 1563 (1993).
[14] E. E. Meshkov, Proceedings of the Ninth All-Russian Symposium on Applied and Theoretical Mechanics, Nizhnii Novgorod, Russia, 22–28 August 2006 (unpublished), Chap. 2, p. 132.
[15] K. S. Vecchio, U. Andrade, M. A. Meyers, and L. W. Meyer, in *Shock Compression of Condensed Matter-1991*, edited by S. C. Schmidt, R. D. Dick, J. W. Forbes, and D. G. Tasker (Elsevier Science, Amsterdam, 1991), pp. 527–530, Paper No. QC 173.4 C65A43.
[16] A. H. Chokshi and M. A. Meyers, Scr. Metall. **24**, 605 (1990).
[17] J. E. Flinn, G. E. Duvall, G. R. Fowles, and R. F. Tinder, J. Appl. Phys. **46**, 3752 (1975).
[18] P. Kumar and R. J. Clifton, J. Appl. Phys. **48**, 4747 (1979).
[19] W. F. Hartman, J. Appl. Phys. **35**, 2090 (1964).
[20] M. D. Funish, W. M. Trott, J. Mason, J. Podsednik, W. D. Reinhart, and C. Hall, in *Shock Compression of Condensed Matter-2003*, AIP Conf. Proc. No. 706, edited by M. D. Furnish, Y. M. Gupta, and J. W. Forbes (AIP, Melville, NY, 2004), pp. 1159–1162.
[21] Yu. I. Mescheryakov and A. K. Divakov, Dymat Journal **1**, 271 (1994).
[22] J. R. Asay and L. M. Barker, J. Appl. Phys. **45**, 2540 (1974).
[23] L. W. Morland, Philos. Mag. **251**, 341 (1959).
[24] G. R. Fowles, J. Appl. Phys. **32**, 1475 (1961).
[25] G. V. Stepanov, *Elastic-Plastic Deformation and Fracture of Materials under Pulse Loading* (Naukova Dumka, Kiev, 1991).
[26] D. E. Grady, in *Metallurgical Applications of Shock Wave and High-Strain Phenomena (Exlomet-85)*, edited by L. E. Murr, K. P. Staudhammer, and M. A. Meyers (Dekker, New York, 1986), pp. 763–780.
[27] G. I. Kanel, S. V. Rasorenov, and V. E. Fortov, *Shock-Wave Phenomena and the Properties of Condensed Matter*, edited by L. Davison and Y. Horie (Springer, New York, 2004), Paper No. QC173.454.K36.
[28] J. J. Gilman, in *Shock Compression of Condensed Matter-2001*, AIP Conf. Proc., edited by M. D. Furnish, N. N. Thadhani, and Y. Horie (AIP, Melville, NY, 2002), p. 36.
[29] P. V. Makarov, Phys. Mesomech. **8**, 39 (2005).
[30] J. W. Taylor and M. H. Rice, J. Appl. Phys. **34**, 364 (1963).
[31] L. M. Barker and R. E. Hollenbach, J. Appl. Phys. **45**, 4872 (1974).
[32] G. I. Taylor and H. Quinney, Proc. R. Soc. London, Ser. A **163**, 157 (1937).
[33] M. B. Bever, D. L. Holt, and A. L. Titchener, Prog. Mater. Sci. **17**, 1 (1973).
[34] G. Ravichandran, A. J. Rosakis, J. Hodowany, and P. Rosakis, in *Shock Compression of Condensed Matter-2001*, AIP Conf. Proc. No. 620, edited by M. D. Furnish, N. N. Thadhani, and Y. Horie (AIP, Melville, NY, 2002), pp. 557–562.
[35] T. Nicholas, *Impact Dynamics* (Wiley, New York, 1982), pp. 198–256.
[36] L. D. Landay, E. M. Lifshits. *Hydrodynamics* (Nauka, Moscow, 1988), p. 733.
[37] Yu. I. Meshcheryakov, in *High-Pressure Shock Compression of Solids VI*, edited by Lee Davison and Yashi-Yuki Horie (Springer-Verlag, New York, 2003), pp. 169–213.
[38] Yu. I. Meshcheryakov, in *Shock Compression of Condensed Matter-1999*, AIP Conf. Proc. No. 505, edited by M. D. Furnish, L. C. Chhabildas and R. S. Nixon (AIP, Melville, NY, 2000), pp. 1065–1070.
[39] T. Mura, Philos. Mag. **8**, 843 (1963).
[40] T. Kihara and O. Aono, J. Phys. Soc. Jpn. **8**, 837 (1963).
[41] V. I. Vladimirov, V. I. Nikolaev, and N. M. Priemsky, in *Physics of Strength and Plasticity*, edited by S. I. Zhurkov (Nauka, Leningrad, 1986), pp. 69–80.
[42] J. D. Eshelby, Phys. Rev. **90**, 248 (1953).
[43] F. R. N. Nabarro, Proc. R. Soc. London, Ser. A **209**, 278 (1951).
[44] J. Hubburd, Proc. R. Soc. London, Ser. A **260**, 114 (1961).
[45] J. De Angelis and J. B. Cohen, J. Met. **15**, 681 (1963).